Localised Forced Ignition of Pulverised Coal Particle-laden Mixtures: A Direct Numerical Simulation Analysis

Tamir Brosh, Dipal Patel, Daniel Wacks, Nilanjan Chakraborty
School of Mechanical and System Engineering, Newcastle University
Newcastle Upon Tyne, NE1 7RU, UK
tamir.brosh@ncl.ac.uk; d.patel2@ncl.ac.uk;daniel.wacks@ncl.ac.uk; nilanjan.chakraborty@ncl.ac.uk

Abstract - Localised ignition of mono-disperse pulverised coal particle-laden mixtures has been analysed based on three-dimensional Direct Numerical Simulations with simplified chemistry for the combustion of volatile gases. The coal particles were treated as point sources and tracked in a Lagrangian manner. The coupling between Eulerian gaseous and Lagrangian particulate phases was achieved by appropriate source terms in the mass, momentum, energy and species conservation equations. A detailed parametric analysis was carried out to analyse the effects of particle equivalence ratio Φ_p, root-mean-square turbulent velocity fluctuation u' and particle diameter a_p on self-sustained combustion following successful ignition. An increase in Φ_p has an adverse effect on self-sustained combustion, whereas a reduction in particle size may have detrimental effects on the extent of burning. It was found that an increase in u' increases the rate of mixing of devolatilised fuel with the surrounding air, which though beneficial, for self-sustained combustion, augments the heat transfer rate from the hot gas kernel, thus leading to flame extinction for high values of u'. Detailed physical explanations were provided to explain the observed effects of Φ_p, root-mean-square turbulent velocity fluctuation u' and particle diameter a_p on self-sustained combustion of coal particle-laden mixtures.

Keywords: Direct Numerical Simulation, Coal Combustion, Localised forced ignition, Root-mean-square turbulent velocity fluctuation, Particle-laden mixtures.

1. Introduction

Improved fundamental understanding of coal combustion is necessary for the purpose of designing new generation energy-efficient and environment-friendly boilers and furnaces. However, it is often difficult to obtain detailed experimental data due to practical limitations in the hostile coal combustion environment. A number of analyses have used Reynolds Averaged Navier Stokes (RANS) and Large Eddy Simulations (LES) for analysing coal combustion (Guo *et al.*, 2003; Maldonado *et al.*, 2006; Bermudez *et al.*, 2010; Stein *et al.*, 2013). Guo *et al.* (2003) used a two-fluid model to describe coal particles. Several subsequent analyses (Maldonado *et al.*, 2006; Bermudez *et al.*, 2010; Stein *et al.*, 2013; Hashimoto *et al.*, 2012; Franchetti *et al.*, 2013) used Lagrangian tracking of the coal particles. Recently Luo *et al.* (2012) carried out Direct Numerical Simulations (DNS) of a turbulent jet involving coal particle-laden mixtures where the volatile gas released by coal was modelled as methane CH_4. They considered the coal-particles as point sources and tracked them in a Lagrangian manner. The same approach has been adopted here for the analysis of localised forced ignition of turbulent pulverised coal suspension. It has been found that root-mean-square (rms) turbulent velocity fluctuation u' and equivalence ratio of the mixture Φ at the ignitor location significantly affect the ignition probability and early stages of flame propagation in the case of successful ignition (Mastorakos, 2008). Moreover, the overall equivalence ratio (liquid+gaseous phase), droplet diameter and pre-evaporation turbulence have significant influences on localised ignition of turbulent droplet-laden mixtures (Wandel *et al.*, 2009). Thus, it can be expected that background turbulence, particle equivalence ratio (Φ_p), particle diameter and devolatilisation characteristics will all have major influences on localised ignition of pulverised coal particles. The main objective of the current DNS based analysis is to demonstrate the effects of particle

diameter, particle equivalence ratio and rms turbulent velocity fluctuation on localised ignition and subsequent combustion for coal particle-laden mixtures.

2. Mathematical Background & Numerical Implementation

It is extremely computationally expensive to simultaneously account for both three-dimensionality of turbulence and detailed chemical mechanism especially for particle-laden flows (Luo et $al.$, 2012). Thus the volatile matter released by coal was taken to be CH_4 instead of $C_xH_yO_z$ for the purpose of computational economy following several previous analyses (e.g. Yu et $al.$, 2009; Luo et $al.$, 2012). Here a two-step chemistry (Bibrycki et $al.$, 2010) was considered for CH_4-air combustion, which involves the oxidation reactions for CH_4 and CO (i.e. $CH_4 + 1.5O_2 = CO + 2H_2O$ and $CO + 0.5O_2 = CO_2$) and dissociation of CO_2 (i.e. $CO_2 = CO + 0.5O_2$). The mechanism was calibrated to result in a realistic unstrained laminar burning velocity $S_{(\Phi)}$ variation with equivalence ratio Φ especially for fuel-rich mixtures. The equivalence ratio Φ is defined as $\Phi = AFR_{st}\xi/(1-\xi)$ where AFR_{st} is the stoichiometric air-fuel ratio based on $CH_4 + 2O_2 = CO_2 + 2H_2O$. The mixture fraction ξ is defined based on elemental carbon mass fraction Y_{Cf} arising from primary and secondary fuels (i.e. for CH_4 and CO) as: $\xi = (Y_{Cf} - Y_O/s + Y_{O\infty}/s)/(Y_{Cf\infty} + Y_{O\infty}/s)$ where Y_{Cf} and Y_O are the local carbon mass fraction in fuel and oxygen mass fractions, and $Y_{Cf\infty} = 0.75$ ($Y_{O\infty} = 0.233$) is the elemental carbon (oxygen) mass fraction in the pure methane (air) stream and $s = 5.33$ is ratio of mass of oxygen to the mass of carbon in methane for the stoichiometric mixture (i.e. $\Phi = 1$ and $\xi_{st} = 0.055$). The Lagrangian transport equations for coal particles take the following form (Ubhayakar et $al.$, 1977; Luo et $al.$, 2012):

$$d\vec{x}_p/dt = \vec{v}_p \tag{1i}$$

$$d\vec{v}_p/dt = 18C_d\mu_g(\vec{u} - \vec{v}_p)/\rho_p a_p{}^2 \tag{1ii}$$

$$dm_p/dt = \dot{m}_v + \dot{m}_{ch} \tag{1iii}$$

$$\rho_p(\pi a_p{}^3/6)C_c(dT_p/dt) =$$
$$\pi a_p{}^3(q'''_{rad})_p + (\pi a_p)\mu_g Nu_p C_{pg}(T_g - T_p) + \dot{m}_{v1}h_{v1} + \dot{m}_{v2}h_{v2} + \dot{m}_{chA}h_{chA} + \dot{m}_{chB}h_{chB} + \dot{m}_{chC}h_{chC} \tag{1iv}$$

where $\vec{x}_p$, $\vec{v}_p$, T_p and a_p are location vector, velocity vector, temperature and diameter of an individual particle P respectively, and the radiation heat flux is simplified as $(q''_{rad})_p = \varepsilon_p\sigma(T_{eff}^4 - T_p^4)$ following Luo et $al.$ (2012) where σ is the Stefan-Boltzmann constant and ε_p is the emissivity of the particle, which is taken to be 1.0 here. The density of particle phase, specific heat of coal and viscosity of the gaseous phase are given by ρ_p , C_c and μ_g respectively. The drag coefficient C_d and particle Nusselt number Nu_p are given by $C_d = (24/Re_p)(1 + Re_p^{0.687})$ and $Nu_p = 2 + 0.6Re_p^{0.5}Pr_g^{0.33}$ respectively where $Re_p = \rho_g|\vec{u} - \vec{v}_p|a_p/\mu_g$ is the particle Reynolds number. In eq. 1iii, $\dot{m}_v$ and $\dot{m}_{ch}$ refer to devolatilisation and char reaction rates. For the present analysis the coal particles are taken to be moisture-free and are made up of 23.4% volatile, 39.1% fixed carbon and 37.5% ash based on a typical proximate analysis (Luo et $al.$, 2012). The devolatilisation process can be expressed as (Kobayashi et $al.$, 1977; Luo et $al.$, 2012):

$$coal {\nearrow (1-\alpha_1)R_1 + \alpha_1 V_1 \atop \searrow (1-\alpha_2)R_2 + \alpha_2 V_2} \tag{2}$$

where R_1 and R_2 (V_1 and V_2) indicate residual chars (volatile matters) respectively and $\alpha_1 = 0.234$ and $\alpha_2 = 0.8$ are taken here. The devolatilisation rate $\dot{m}_v$ is expressed as (Kobayashi et $al.$, 1977; Luo et $al.$, 2012): $\dot{m}_v = \dot{m}_{v1} + \dot{m}_{v2} = -\alpha_1 m_{daf}B_{v1}\exp(-E_{v1}/RT_p) - \alpha_2 m_{daf}B_{v2}\exp(-E_{v2}/RT_p)$ where m_{daf} is the dry ash free mass and the pre-exponential factors (PEFs), B_{v1} and B_{v2}, and activation energies (AEs), E_{v1} and E_{v2}, and the enthalpies h_{v1} and h_{v2} are taken from Kobaayashi et $al.$(1977). The char-reaction

rate is expressed as: $\dot{m}_{ch} = \dot{m}_{chA} + \dot{m}_{chB} + \dot{m}_{chC}$ where $\dot{m}_{chA} = (1 - \beta_{chA})\pi a_p{}^2 Y_{O_2,s}\rho_s B_{chA}\exp(-E_{chA}/RT_p)$, $\dot{m}_{chB} = (1 - \beta_{chB})\pi a_p{}^2 Y_{O_2,s}\rho_s B_{chB}\exp(-E_{chB}/RT_p)$ and $\dot{m}_{chC} = (1 - \beta_{chC})\pi a_p{}^2 Y_{CO_2,s}\rho_s B_{chC}\exp(-E_{chC}/RT_p)$ are associated with the reactions $C + O_2 \rightarrow CO_2$, $2C + O_2 \rightarrow 2CO$ and $C + CO_2 \rightarrow 2CO$ respectively and the mass fraction of O_2 and CO_2 on the coal surface are given by $Y_{O_2,s}$ and $Y_{CO_2,s}$ respectively, which are evaluated using an iterative procedure based on the total mass flow from/to the particle and β_{chA}, β_{chB} and β_{chC} are the stoichiometric ratio of char oxidation on the particle surface. The PEFs (B_{chA}, B_{chB} and B_{chC}), enthalpies of char oxidation (h_{chA}, h_{chB} and h_{chC}), and AEs (E_{chA}, E_{chB} and E_{chC}) are taken according to Ubhayakar *et al.* (1977). The quantities $Y_{O_2,s}$ and $Y_{CO_2,s}$ are evaluated based on mass flow rates obtained from reactions: $\dot{m}_{O_2} = \beta_{chA}\dot{m}_{chA} + \beta_{chB}\dot{m}_{chB}$, $\dot{m}_{CO_2} = -(1 + \beta_{chA})\dot{m}_{chA} + \beta_{chC}\dot{m}_{chC}$ and $\dot{m}_{CO} = -(1 + \beta_{chB})\dot{m}_{chB} - (1 + \beta_{chC})\dot{m}_{chC}$ in the following manner (Ubhayakar *et al.*, 1977; Luo *et al.*, 2012):

$$Y_{O_2,s} = -(\dot{m}_{O_2}/\Sigma\dot{m}_p) + (Y_{O_2,g} + \dot{m}_{O_2}/\Sigma\dot{m}_p)\exp[-|\Sigma\dot{m}_p|C_{PS}/(\pi a_p \lambda_s Nu_p)] \tag{3i}$$

$$Y_{CO_2,s} = -(\dot{m}_{CO_2}/\Sigma\dot{m}_p) + (Y_{CO_2,g} + \dot{m}_{CO_2}/\Sigma\dot{m}_p)\exp[-|\Sigma\dot{m}_p|C_{PS}/(\pi a_p \lambda_s Nu_p) \tag{3ii}$$

where $\Sigma\dot{m}_p = \dot{m}_{v1} + \dot{m}_{v2} + \dot{m}_{O_2} + \dot{m}_{CO_2} + \dot{m}_{CO}$ is the net mass flow rate associated with the particle, C_{PS} and λ_s are the specific heat and thermal conductivity around the coal particle. The coupling between mass, momentum, energy and species conservation equations between the dispersed and carrier phases is obtained by introducing source terms due to dispersed phase in the Eulerian phase transport equations in the following manner (Wandel *et al.*, 2009; Hashimoto *et al.*, 2012; Luo *et al.*, 2012; Stein *et al.*, 2013; Franchetti *et al.*, 2013):

$$\partial(\rho_g\varphi)/\partial t + \partial(\rho_g u_j\varphi)/\partial x_j = \nabla \cdot [(\mu_g/\sigma_\varphi)\nabla\varphi] + \dot{S}_{\varphi g} + \dot{S}_{\varphi p} + \dot{S}_{\varphi ch} \tag{4}$$

where φ is a general primitive variable, ρ_g is the gas density, σ_φ is the Schmidt number associated with φ and the source terms $\dot{S}_{\varphi g}$ and $\dot{S}_{\varphi p}$ arise from gaseous and dispersed phases respectively. The variable φ is equal to 1 for mass conservation, u_i for momentum conservation in the ith direction, specific internal energy $e = \int_{T_{ref}}^{\hat{T}} C_{vg}dT + (u_k u_k/2)$ for energy conservation and Y_α for conservation of species α, where $\hat{T}$ and T_{ref} are the instantaneous gas and reference temperatures respectively. The particle source term $\dot{S}_{\varphi p}$ is evaluated as (Wandel *et al.*, 2009; Hashimoto *et al.*, 2012; Luo *et al.*, 2012; Stein *et al.*, 2013; Franchetti *et al.*, 2013):

$$\dot{S}_{\varphi p} = -(\Delta V)^{-1}\sum_p d(m_p\varphi_p)/dt \tag{5}$$

where ΔV is the volume of the cell and the summation is over all the coal particles in the vicinity of a given node. The source term due to char combustion $\dot{S}_{\varphi ch}$ appears only in the transport equations for the mass fractions of O_2, CO and CO_2 and they are evaluated using an expression similar to eq. 5 where the mass flow rates are evaluated using char reaction rates. The heat addition by the ignitor is accounted for by a source term $q'''(r) = A_q \cdot \exp(-r^2/2R^2)$ in the energy transport equation where r is the radial direction from the centre of the ignitor (Wandel *et al.*, 2009) and R is taken to be $1.73l_f$ where $l_f = D_0/S_{b(\Phi=1)}$ is the Zel'dovich flame thickness for the stoichiometric mixture where D_0 is the mass diffusivity in the unburned gas and $S_{b(\Phi=1)}$ is the unstrained laminar burning velocity of the stoichiometric mixture of volatile fuel and air. The parameter A_q is determined by: $\dot{Q} = \int_V q'''dV$ where $\dot{Q}$ is the ignition power, which is defined as (Wandel *et al.*, 2009): $\dot{Q} = a_{sp}\rho_0 C_P\tau T_0(4\pi l_f^3/3)[H(t - t_1) - H(t - t_2)]/(t_2 - t_1)$ where $\tau = (T_{ad(\Phi=1)} - T_0)/T_0$ is the heat

release parameter (where $T_{ad(\Phi)}$ and T_0 are the adiabatic flame temperature for equivalence ratio Φ and the unburned gas temperature respectively) and a_{sp} is a parameter that determines the energy deposition by the ignitor and is taken to be $a_{sp} = 25.72$ in the current analysis. The time instants t_1 and t_2 determine the duration $t_{sp} = (t_2 - t_1) = b_{sp}t_F$ over which the energy is deposited by the ignitor, where b_{sp} is a duration parameter and t_F is the chemical time scale given by $t_F = l_f/S_{b(\Phi=1)}$. In the present study, b_{sp} is taken to be 0.2 following Wandel *et al.* (2009).

The DNS simulation domain was taken as $33l_f \times 33l_f \times 33l_f$, which was discretised using a uniform Cartesian grid of $200 \times 200 \times 200$. This grid spacing ensures 10 grid points within the thermal flame thickness of the stoichiometric mixture $\delta_{th} = (T_{ad(\Phi=1)} - T_0)/\max|\nabla\hat{T}|_L$ and the subscript L refers to the unstrained laminar premixed flame quantities for the stoichiometric methane-air mixture. The boundaries in the x_1 direction were taken to be partially non-reflecting. The boundaries in the other directions were considered to be periodic. High order central-difference and Runge-Kutta methods were used for spatial differentiation and time advancement respectively. The mono-dispersed, preheated (=550K) coal particles were randomly distributed in the domain in x_2 and x_3 directions and over the 70% of the domain length in the x_1 direction around the centre of the domain. The values associated with parametric variations of rms turbulent velocity fluctuation u', particle radius a_p and particle equivalence ratio Φ_p are summarised in Table 1. The initial values of the normalised turbulent velocity fluctuation $u'/S_{b(\Phi=1)}$, , normalised particle diameter a_p/l_f and particle equivalence ratio Φ_p are also listed in Table 1. The ratio of longitudinal integral length scale to flame thickness L_{11}/l_f is taken to be 5.2 (i.e. $L_{11}/l_f = 5.2$) for turbulent cases. The heat release parameter $\tau = (T_{ad(\Phi=1)} - T_0)/T_0$ is taken to be 3.0 for all cases considered here. Standard values are taken for the ratio of specific heats ($\gamma = C_P/C_V = 1.4$) and Prandtl number (Pr = 0.7). For the base (reference) case b the Kolmogorov length scale η remains 1.86 times of the grid spacing (i.e. $\eta \approx 1.86\Delta x$). All simulations have been carried out at the least for $t = 10t_{sp} = 2.0t_F$, which corresponds to about $1.47t_e$, $1.96t_e$ and $3.92t_e$ for initial values of $u'/S_{b(\Phi=1)} = 3, 4$ and 8 respectively where $t_e = L_{11}/\sqrt{k}$ is the initial eddy turn over time.

Table 1. Parametric variation and base case.

Base case (b)		Parametric variation		
$a_{p,b} = 0.12l_f$	$\dfrac{a_p}{a_{p,b}}$	0.5	a$_1$	
		1.0	b	
		1.5	a$_2$	
$\Phi_{p,b} = 1.0$	$\dfrac{\Phi}{\Phi_{p,b}}$	0.5	P$_1$	
		1.0	b	
		2.0	P$_2$	
		3.0	P$_3$	
$\dfrac{u'_b}{S_{b(\Phi=1)}} = 4.0,\ \dfrac{L_{11}}{l_f} = 5.2$	$\dfrac{u'}{u'_b}$	0	L	
		0.75	U$_1$	
		1.0	b	
		2.0	U$_2$	

4. Results and Discussions

The variations of the maximum non-dimensional temperature, $T_{\max}$, and the normalised total devolatilisation rate from the particles, $\Sigma(\dot{m}_v)_p/\rho_0 l_f^2 S_{b(\Phi=1)}$, for cases P$_1$, b, P$_2$ and P$_3$ with $a_p/a_{p,b} = 1.0$ and $u'/u'_b = 1.0$ are shown in Fig. 1 where $T_{\max} = (\hat{T} - T_0)/(T_{ad(\Phi=1)} - T_0)$ is the non-

dimensional temperature. Figure 1 shows that T_{max} rises due to deposition of energy, which in turn increases the temperature of the coal particles leading to devolatilisation of volatile matter. The number of coal particles affected by the external deposition of energy during the ignition phase increases with increasing Φ_p. The devolatilisation rate increases with the rise of temperature of the coal particles and the availability of greater amount of combustible devolatilised gas at higher value of Φ_p gives rise to stronger thermal runaway, which is reflected in the higher values of T_{max} at $t = t_{sp}$. Once the ignitor is switched off T_{max} begins to drop, but the coal particles continue to absorb heat from the surrounding hot gas thus the devolatilisation rate continues to rise. The amount of volatile gas released by the coal particles is relatively small for small values of Φ_p. The equivalence ratio of fuel-air mixture next to the coal particles is typically too high to support combustion. Thus, the released volatile gas needs to diffuse from devolatilisation sites to obtain ξ values which are close to the most reactive mixture fraction ξ_{MR} so that autoignition of volatile gas can take place due to high surrounding temperature (Mastorakos *et al.*, 1997). This autoignition leads to the second peak in T_{max} at $t > t_{sp}$ for case P_1 in Fig. 1. The temporal evolution of the maximal reaction rate magnitude for primary fuel (methane), $|\dot{w}_F|_{max} \times l_f / \rho_0 S_{b(\Phi=1)}$, for cases P_1,b, P_2 and P_3 for $a_p/a_{p,b} = 1.0$ and $u'/u'_b = 1.0$ is also presented in Fig. 1. The reaction rate magnitude increases rapidly with time during the ignition period (i.e. $t \leq t_{sp}$) once sufficient volatile fuel mixes with the surrounding air to form a gaseous flammable mixture. The high rate of heat transfer from the hot gas kernel due to the high temperature gradient between the ignition kernel and the surrounding air leads to a reduction in the maximum temperature T_{max} with time when the ignitor is switched off, which also gives rise to reduction in $|\dot{w}_F|_{max} \times l_f / \rho_0 S_{b(\Phi=1)}$ with time, but the variations of T_{max} and $|\dot{w}_F|_{max} \times l_f / \rho_0 S_{b(\Phi=1)}$ with time eventually slow down and do not appreciably change with time for $t \gg t_{sp}$ for self-sustained combustion. In the case of self-sustained combustion T_{max} settles to a value close to, but slightly smaller than, the adiabatic flame temperature of the stoichiometric mixture (i.e. $T_{max} \approx 1.0$) due to incomplete burning of volatile matter. Figures 1a-c show that $\Sigma(\dot{m}_v)_p / \rho_0 l_f^2 S_{b(\Phi=1)}$ rises even when T_{max} and $|\dot{w}_F|_{max} \times l_f / \rho_0 S_{b(\Phi=1)}$ decrease with time for $t_{sp} \leq t \leq 5t_{sp}$ ($t_{sp} \leq t \leq 4t_{sp}$) in cases P_1 and b (cases P_2 and P_3) for $a_p/a_{p,b} = 1.0$ and $u'/u'_b = 1.0$, but $\Sigma(\dot{m}_v)_p / \rho_0 l_f^2 S_{b(\Phi=1)}$ approaches to a weakly time-dependent value for $t \gg t_{sp}$ (e.g. $8t_{sp} \leq t \leq 10t_{sp}$) for the cases where self-sustained combustion is obtained. Too much devolatilisation at early stages of ignition for high values of Φ_p may lead to regions of fuel-rich non-combustible gaseous mixtures, which is detrimental to the possibility of obtaining self-sustained combustion following a successful ignition. This is substantiated by the continuous drop in T_{max} and $|\dot{w}_F|_{max} \times l_f / \rho_0 S_{b(\Phi=1)}$ with time for cases P_3 with $a_p/a_{p,b} = 1.0$ and $u'/u'_b = 1.0$ for $t \gg t_{sp}$ (see the variations during $7t_{sp} \leq t \leq 10t_{sp}$), which also leads to eventual drop in $\Sigma(\dot{m}_v)_p / \rho_0 l_f^2 S_{b(\Phi=1)}$.
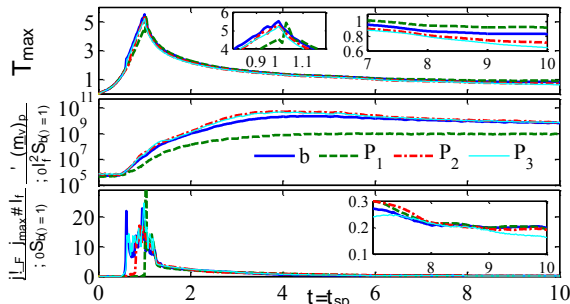
Fig. 1. The temporal variation of T_{max}, $\Sigma(\dot{m}_v)_p / \rho_0 l_f^2 S_{b(\Phi=1)}$ and $|\dot{w}_F|_{max} \times l_f / \rho_0 S_{b(\Phi=1)}$ with $u'/u'_b = 1.0$ and $a_p/a_{p,b} = 1.0$.
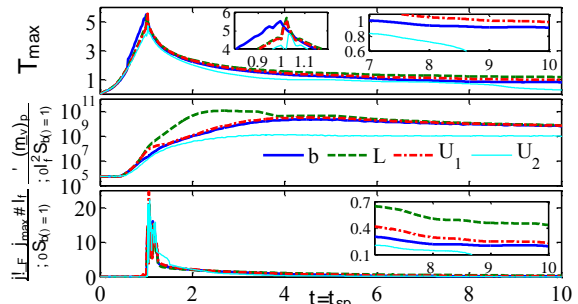
Fig. 2. The temporal variation of T_{max}, $\Sigma(\dot{m}_v)_p / \rho_0 l_f^2 S_{b(\Phi=1)}$ and $|\dot{w}_F|_{max} \times l_f / \rho_0 S_{b(\Phi=1)}$ with $\Phi_p/\Phi_{p,b} = 1.0$ and $a_p/a_{p,b} = 1.0$.

The temporal variations of $T_{\max}$, $\Sigma(\dot{m}_v)_p/\rho_0 l_f^2 S_{b(\Phi=1)}$ and $|\dot{w}_F|_{\max} \times l_f/\rho_0 S_{b(\Phi=1)}$ for cases L, U_1, b and U_2 are shown in Fig. 2 for $\Phi_p/\Phi_{p,b} = 1.0$ and $a_p/a_{p,b} = 1.0$. An increase in u' augments the heat transfer rate from the hot gas kernel which reduces the volume of the hot gas kernel. Thus, the number of particles, affected by high temperature gas, decreases with increasing u'. This leads to a decrease in $\Sigma(\dot{m}_v)_p/\rho_0 l_f^2 S_{b(\Phi=1)}$ with increasing u', which along with the augmented heat transfer from hot gas kernel may lead to failure of self-sustained combustion for high values of u'. For example, for $\Phi_p/\Phi_{p,b} = 1.0$ and $a_p/a_{p,b} = 1.0$, self-sustained combustion fails in case U_2, whereas self-sustained combustion has been obtained following successful ignition in cases L, U_1 and b. The detrimental effects of u' on early stages of combustion following localised ignition of coal particle-laden mixtures is consistent with previous analyses involving inhomogeneous gaseous (Mastorakos, 2008) and droplet-laden (Wandel *et al.*, 2009) mixtures.

The temporal variations of $T_{\max}$, $\Sigma(\dot{m}_v)_p/\rho_0 l_f^2 S_{b(\Phi=1)}$ and $|\dot{w}_F|_{\max} \times l_f/\rho_0 S_{b(\Phi=1)}$ for cases a_1, b and a_2 are presented in Fig. 3 for $u'/u_b' = 1.0$ and $\Phi_p/\Phi_{p,b} = 1.0$, in which case a_2 exhibits smaller value of $\Sigma(\dot{m}_v)_p/\rho_0 l_f^2 S_{b(\Phi=1)}$ and higher values of $|\dot{w}_F|_{\max} \times l_f/\rho_0 S_{b(\Phi=1)}$ at early stages of combustion following successful ignition (e.g. $|\dot{w}_F|_{\max} \times l_f/\rho_0 S_{b(\Phi=1)}$ assumes greater values in case a_2 than case b during $t_{sp} \leq t \leq 6t_{sp}$). The smaller rate of devolatilisation in case b than in case a_1 reduces the probability of obtaining non-combustible fuel-rich mixture for $u'/u_b' = 1.0$ and $\Phi_p/\Phi_{p,b} = 1.0$, which in turn leads to higher value of $|\dot{w}_F|_{\max} \times l_f/\rho_0 S_{b(\Phi=1)}$ in case b than in case a_1 during early stages of combustion following successful ignition. The rate of devolatilisation is greater (smaller) for cases with smaller (larger) particle size, such as case a_1 (case a_2), which leads to high probability of finding localised pockets of highly fuel-rich non-combustible mixtures for cases with small particle sizes. The reduction in surrounding gas temperature has a more pronounced effect for smaller particles, which eventually reduces devolatilisation rate in these cases. At $t \gg t_{sp}$ devolatilisation rate from particles in cases a_1, b and a_2 takes place at a rate which is sufficient to sustain combustion without any external energy addition.
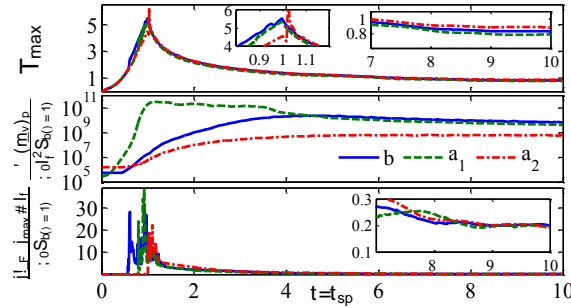
Fig. 3. The temporal variation of $T_{\max}$, $\Sigma(\dot{m}_v)_p/\rho_0 l_f^2 S_{b(\Phi=1)}$ and $|\dot{w}_F|_{\max} \times l_f/\rho_0 S_{b(\Phi=1)}$ with $u'/u_b' = 1.0$ and $\Phi_p/\Phi_{p,b} = 1.0$.

The extent of burning can be quantified in the form of total mass of CO, CO_2 and H_2O (i.e. $m_{CO} + m_{CO_2} + m_{H_2O}$) produced due to combustion of volatile fuel. The temporal evolutions $(m_{CO} + m_{CO_2} + m_{H_2O})/([4/3]\rho_0\pi l_f^3)$ are shown in Fig. 4 for different values of Φ_p, u' and a_p. Figure 4 shows that smaller values of $(m_{CO} + m_{CO_2} + m_{H_2O})$ are obtained for higher values of Φ_p because the probability of finding highly fuel-rich non-combustible mixture increases with Φ_p, which in turn reduces the extent of burning for high values of Φ_p. It can be seen from Fig. 4 that $(m_{CO} + m_{CO_2} + m_{H_2O})$ does not change with time for high values of u' (e.g. case U_2) indicating cessation of combustion of volatile fuel due to failure of self-sustained combustion. For high values of u' (e.g. case U_2) the heat transfer from hot gas kernel overcomes the chemical heat release, which reduces the temperature of the hot gas kernel to such an extent that it gives rise to insufficient devolatilisation rate, leading to the

unavailability of sufficient gaseous fuel and weak chemical heat release to maintain self-sustained combustion in the absence of external energy addition. Figure 4 further shows that for the quiescent (i.e. $u' = 0$) case, $(m_{CO} + m_{CO_2} + m_{H_2O})$ increases continuously with time, but the values of $(m_{CO} + m_{CO_2} + m_{H_2O})$ remain smaller than in the turbulent cases where self-sustained combustion has been obtained (e.g. cases U_1 and b) for $\Phi_p = 0.5$, 1 and 2, and the values of $(m_{CO} + m_{CO_2} + m_{H_2O})$ for cases L and b are comparable to the corresponding values for $\Phi_p = 3.0$ at $t \gg t_{sp}$. In turbulent cases, the volatile gas from the high fuel-rich sites next to the particles diffuses more rapidly to produce a flammable mixture, in comparison to the quiescent cases, due to augmented mixing action in turbulent flows. Thus the probability of finding fuel-rich non-combustible mixtures is higher in the quiescent case than in cases U_1 and b, which leads to smaller values of $(m_{CO} + m_{CO_2} + m_{H_2O})$ in the quiescent case for $\Phi_p = 0.5$, 1 and 2. An increase in u' helps in mixing the volatile fuel with the surrounding air to produce flammable mixtures but also increases heat transfer rate from the hot gas kernel. The relative strengths of these competing effects are affected by Φ_p and a_p, which in turn determine the extent of burning and the possibility of obtaining self-sustained combustion. The rate of devolatilisation increases with decreasing particle diameter, and the high rate of devolatilisation for the small particles leads to a high probability of finding fuel-rich non-combustible mixtures, which reduces the extent of burning. This is reflected in the higher value of $(m_{CO} + m_{CO_2} + m_{H_2O})$ in case a_2 (case b) than in case b (case a_1). For case P_1, Φ_p is sufficiently low so that the problem of obtaining fuel-rich volatile clouds arising from rapid devolatilisation is not so severe, so $(m_{CO} + m_{CO_2} + m_{H_2O})$ assumes values, which are comparable to the corresponding values in cases b and a_2. Smaller particles introduce more volatile gas into the gaseous phase, which in turn produces high probability of finding fuel-rich non-combustible mixture for high values of Φ_p. Therefore, small values of $(m_{CO} + m_{CO_2} + m_{H_2O})$ for cases with small a_p are more pronounced for high values of Φ_p.
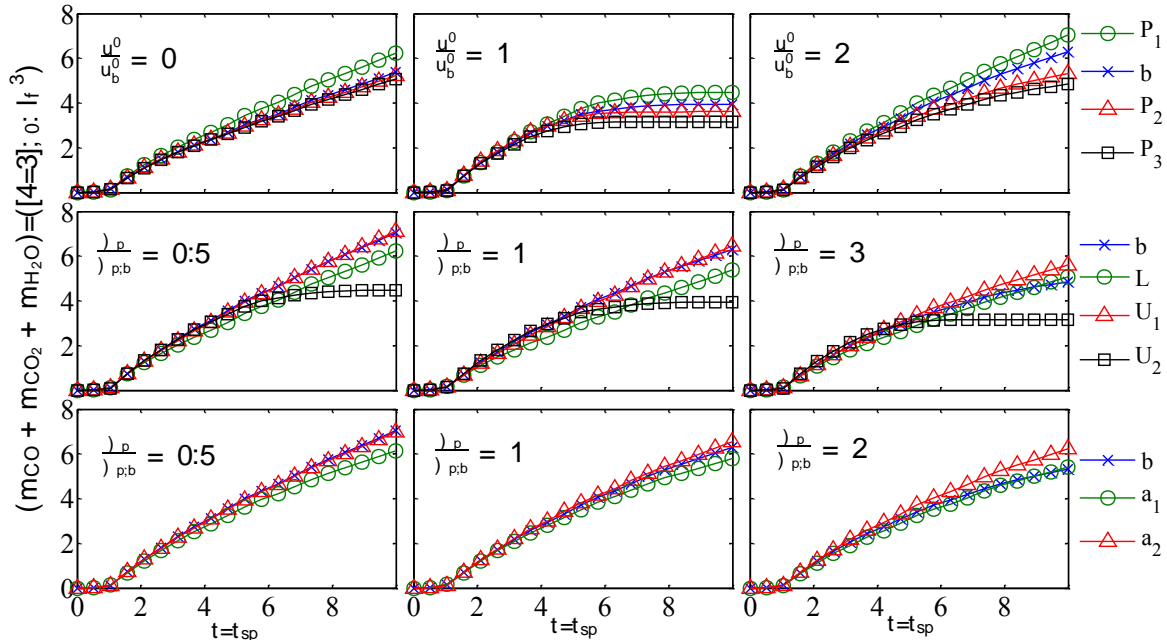
Fig. 4. Temporal evolution of $(m_{CO} + m_{CO_2} + m_{H_2O})\big/([4/3]\rho_0\pi l_f^3)$ for different values of Φ_p, $u'/S_{b(\Phi=1)}$ and a_p [1st row - $a_p/a_{p,b} = 1.0$, 2nd row - $a_p/a_{p,b} = 1.0$ and 3rd row - $u'/u_b' = 1.0$].

5. Conclusion

The effects of Φ_p, u' and a_p on localised ignition of pulverised coal particle-laden mixture and early stages of combustion subsequent to successful ignition have been analysed based on three-

dimensional compressible DNS simulations. It has been found that an increase in Φ_p has adverse effects on self-sustained combustion due to the high probability of obtaining fuel-rich non-combustible fuel-air mixture. Turbulent velocity fluctuations help in mixing the volatile matter from sites of devolatilisation with the surrounding air, which is beneficial for self-sustained combustion and leads to higher probability of finding flammable fuel-air mixtures than under quiescent flow conditions. However, the rate of heat transfer overcomes the rate of heat release due to chemical reaction for high values of u', which eventually can lead to flame extinction. The devolatilisation rate increases with decreasing a_p but too rapid devolatilisation gives rise to high probability of obtaining non-combustible fuel-rich mixture which reduces the extent of burning. Although the qualitative nature of the present findings is unlikely to change, simulations with higher Re_t and detailed chemical kinetics will be necessary for more comprehensive understanding.

Acknowledgements

References

Bermudez, A., Ferrın, J. L., Linan, A. and Saavedra, L., Mathematical modelling of pulverized coal furnaces, Monografıas de la Real Academia de Ciencias de Zaragoza, 34 (2010) 27–50.

Bibrycki, J, Poinsot, T., Zajdel, A., Invetigation of laminar flame speed of CH4/N2/O2 and CH4/Co2/O2 mixtures using reduced chemical kinetic mechanisms. *Archivum combustionis*. 30 (2010),. 287-296.

Franchetti, B.M., Cavallo Marincola, F., Navarro-Martinez, S., Kempf, A. M., Large Eddy Simulation of a Pulverised Coal Jet Flame, *Proc. Combust. Inst.*, 34 (2013) 2419–2426.

Guo,Y.C., Chan, C.K., Lau, K.S., Numerical Studies of Pulvesized coal combustion in a tubular coal combustor with slanted oxygen jet, *Fuel*, 82 (2003) 893–907.

Hashimoto, N., Kurose, R., Hwang, S.-M., Tsuji, H., Shirai, H., A numerical simulation of pulverized coal combustion employing a tabulated-devolatilization-process model (TDP) model, *Combust. Flame*, 159 (2012) 353–366.

Kobayashi, H., Howard, J.B., Sarofim, A. F., Coal devolatilization at high temperatures, *Proc. Combust. Inst.*,16 (1977) 411−425.

Luo, K., Wang, H., Fan, J., Yi, F., Direct Numerical Simulation Study of an Experimental Lifted H2/N2 Flame, Part : Validation and Flame Structure, *Energy & Fuels*, 26 (2012) 6128-6136.

Maldonado,D., Zulli, P., Shen, Y.S., Guo, B.Y., Yu, A.B., Rogers, H., Application of a Numerical Model in the Design of Blast Parameters for an Iron making Blast Furnace, Proc. of 5th International Conference on CFD in the Process Industries, CSIRO, Melbourne, Australia, 13-15 December 2006.

Mastorakos, E., Ignition of turbulent non-premixed flames, *Prog. Ener. Combust. Sci.*, 35 (2009) 57-97.

Mastorakos, E., Baritaud, T., Poinsot, T. J., Numerical simulations of autoignition in turbulent mixing flows, *Combust. Flame*, 109 (1997) 198-223.

Stein, O.T., Olenik, G., Kronenburg, A., Cavallo Marincola, F., Franchetti, B.M., Kempf, A. M., Ghiani, M. , Vascellari, M., Hasse, C., Towards comprehensive coal combustion modelling for LES flow, *Turb. And Comb.*, 90 (2013) 859–884.

Ubhayakar, S.K., Stickler, D.B., Gannon, R.E.,Modelling of entrained bed pulverized coal gasifiers, *Fuel*, 56 (1977) 281–291.

Wandel, A.P., Chakraborty, N., Mastorakos, E., Direct Numerical Simulations of turbulent flame expansion in fine sprays, *Proc. Combust. Inst.*, 32 (2009) 2283–2290.

Yu, J., Zhang, M., Zhang, J., Experimental and numerical investigations on the interactions of volatile flame and char combustion of a coal particle, *Proc. Combust. Inst.*, 32 (2009) 2037−3042.